Mechanical Structure for the PSI Canted-Cosine-Theta (CCT) Magnet Program

Giuseppe Montenero, Bernhard Auchmann, Lucas Brouwer, Ciro Calzolaio, Shlomo Caspi, Gabriella Rolando, and Stephane Sanfilippo

***Abstract*—The Canted-Cosine-Theta (CCT) technology has the potential, by its intrinsic stress-management, to lower coil stresses in high-field accelerator magnets. This is especially relevant for Nb_3Sn magnets, which may be subject to irreversible degradation if the coil stresses exceed critical values. The internal structure of CCT coils, however, dilutes the engineering current density. For an efficient design, the internal structure, therefore, needs to be reduced to the limit given by the computer-numerical-control machining capabilities. In that case, however, additional mechanical stiffness must be provided by an external mechanical structure. The mechanical structure for the Paul Scherrer Institut (PSI) CCT program, which is described in this paper, is based on the bladder and key concept. The CCT-specific deviations from the prevalent bladder and key implementations are discussed. In addition, a two-dimensional and three-dimensional analysis in all stages of loading, cooling, and powering of the first PSI magnet prototype, as well as a tolerance analysis, is reported.**

***Index Terms*—Superconducting magnets, accelerator magnets, magnet structure.**

I. Introduction

THE requirements for superconducting magnets in high energy particle accelerators are pushing practical low temperature superconductors (LTS) to their performance limits [1]. In particular, the Future Circular Collider (FCC) study [2] calls for the development of 16 T bending magnets, which is almost twice the field value of Nb-Ti magnets presently installed in the Large Hadron Collider [3] and 6 T above the record value reached with a Nb-Ti dipole magnet [4]. Such a field level demands a shift toward Nb_3Sn technology. However, Nb_3Sn is a brittle and strain sensitive material. In the worst case, high stress on the coils could result in Nb_3Sn filaments to crack and irreversible coil performance degradation. Therefore, limiting the mechanical stress on the coils during operation is of foremost importance. An effective stress-management enables the introduction of mechanical margins in order to avoid the degradation of the superconducting coils' critical properties during operation.

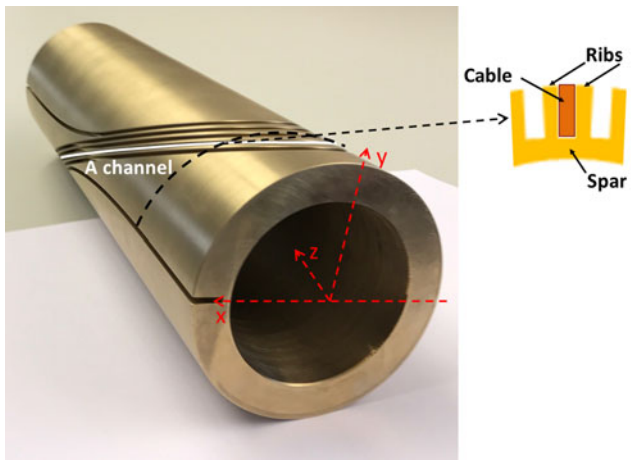

Fig. 1. Example of CCT winding mandrel; (inset) detail of the cross section.

In the framework of the 16 T dipole program for the FCC study [5], three candidate options for a 16 T dipole accelerator magnet, were initially explored [6]–[8]. The initial studies showed the capability of the three designs (Cosine-Theta, Common-Coil, and Block-Coils) to keep the coil stress at the nominal operating current (I_{nom}), below the limit of 200 MPa at 4.2/1.9 K using coil pre-stress techniques [9], with sufficient aperture and field quality. At the same time, the availability of a fourth option, that could in principle provide higher margins through a better stress-management, is of interest for the FCC study. In this regard, the Paul Scherrer Institut (PSI) joined the FCC study proposing a Canted-Cosine-Theta (CCT) design for the 16 T dipole magnet [10]. The development program is carried out in close collaboration with Lawrence Berkeley National Laboratory (LBNL).

CCT technology has the potential, by its intrinsic stress-management, to lower the coil stress in high-field Nb_3Sn accelerator magnets [11]. This capability is provided by the winding mandrel or former. In Fig. 1 an example of a short CCT former is shown. The cable is wound into a channel, along a tilted helical path around the aperture, and each turn is separated through metallic ribs. As a consequence, each turn has an individual azimuthal and axial mechanical support that allows transmit-

Manuscript received August 25, 2017; accepted December 8, 2017. Date of publication December 27, 2017; date of current version January 18, 2018. This work was supported by the Swiss State Secretariat for Education, Research and Innovation SERI. *(Corresponding author: Ciro Calzolaio.)*

G. Montenero, C. Calzolaio, G. Rolando, and S. Sanfilippo are with the Paul Scherrer Institute, Villigen 5232, Switzerland (e-mail: giuseppe.montenero@psi.ch).

B. Auchmann is with the Technology Department, CERN, Geneva CH-1211, Switzerland, and also with the Paul Scherrer Institute, Villigen 5232, Switzerland (e-mail: bernhard.auchmann@cern.ch; bernhard.auchmann@psi.ch).

L. Brouwer and S. Caspi are with the Lawrence Berkeley National Laboratory, Berkeley, CA 94720 USA (e-mail: lnbrouwer@lbl.gov; s_caspi@lbl.gov).

Color versions of one or more of the figures in this paper are available online at http://ieeexplore.ieee.org.

Digital Object Identifier 10.1109/TASC.2017.2787596

ting axial and azimuthal components of Lorentz forces during operation to the internal part of the former, which is called the spar [12]. As for radial forces, the former also aids the coils to make them stiffer. Although this supporting structure is beneficial in terms of stress-management, it reduces the engineering current density of a CCT with respect to classical magnet designs. Therefore, in order to achieve a cost-efficient design, the supporting structure must be reduced down to the limit of the computer-numerical-control (CNC) machining capabilities, while respecting handling and load requirements. Such an optimized former may have a minimal rib thickness of few tenths of a millimeter, and a spar thickness of few millimeters. In this regard, manufacturing trials are envisioned in order to address issues related to distortions during CNC machining; see also [10]. Due to the thin spars and in order to avoid excessive deformation (ovalization) of the former under dipole forces, an additional external mechanical structure is then required. To study these technology challenges, the PSI CCT Program was launched. The main goal is to address key design aspects of an efficient 16 T CCT dipole accelerator magnet.

In this paper, the focus is on the mechanical structure required for the PSI CCT program. The design of an efficient 16 T CCT dipole magnet is covered in an accompanying paper [10]. In the following, Section II outlines the road map of the PSI CCT Program; Section III describes the design of the mechanical structure, to be used in different iterations of technology model magnets; and in Section IV, the mechanical analysis of the first CCT model prototype (CD1) is detailed.

II. The PSI CCT Program

The ultimate goal of the PSI CCT Program is to proof the feasibility of a 16 T CCT dipole accelerator magnet, as a valid alternative to classical designs. The key concepts underlying an efficient CCT dipole design are (i) the minimization of the formers' spar thickness, (ii) the use of thin ribs, and (iii) the use of wide (15 mm) Nb_3Sn cables with large (1 mm) diameter strands in a coil with free-aperture diameter of 50 mm. All these factors contribute to increase in the engineering current density (J_e), rendering the CCT magnet more cost efficient. However, the key concepts set likewise technological challenges. Minimization of the spars' thickness requires the design of an external mechanical support structure for a proper stress-management. The ultimate thickness of a rib depends on the CNC machining capabilities. Wider cables introduce difficulties in terms of coil winding as well as in CNC machining.

The PSI CCT Program is organized to incrementally face those challenges setting out three main activities:

1) Construction of a 1-m-long, 2-layer CCT single-aperture dipole model, called Canted Dipole One (CD1), where the formers have 3-mm-thick spars, 10.6-mm-deep channels, and minimum rib thickness of 0.35 mm. The radial support is guaranteed by an external mechanical structure based on a bladder and key concept, to be described in the following section.
2) Subsequently, construction of a 1-m-long, 2-layer CCT single-aperture dipole model, CD2, where the formers, with 16-mm-deep channels, are optimized to improve the windability for wide Rutherford cables. The spar thickness is reduced to 2 mm and the minimum rib thickness to 0.25 mm. The outer layer of CD2 has the same outer diameter as that of CD1, which allows reusing the external mechanical structure of CD1.
3) Manufacturability improvement and cost reduction of formers for long magnets. This activity is aimed at bolstering the credibility of CCT as an option for a large-scale accelerator such as the FCC.

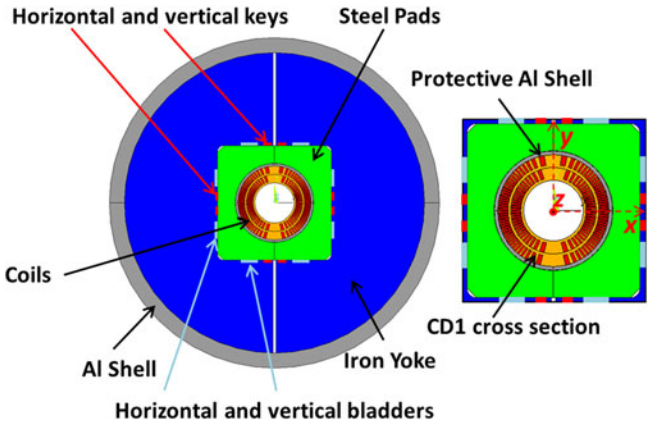

Fig. 2. Left: The proposed bladders-and-keys structure for the PSI CCT program; the coil belongs to the model magnet CD1. Right: Detail coil/pads.

The Nb_3Sn Rutherford cables for the program are based, in the case of CD1, on the CCT R&D cable (strand diameter of 0.85 mm, RRP 108/127 [13], 21 strands) of the US Magnet Development Program (MDP) at LBNL, and, in the case of CD2, on the inner-layer cable of the MDP's 15 T dipole demonstrator, currently being built at FNAL [14] (strand diameter of 1 mm, RRP 150/169 [13], 28 strand).

III. Design of the Mechanical Structure for CCT Model Magnets

As previously stated, a minimal former for a Nb_3Sn high-field CCT dipole magnet does not provide sufficient stiffness to counteract the outward-horizontal dipole forces. During magnet operation, these forces would excessively squeeze the coils toward the midplane (see Fig. 1), leading to plastic deformation of the former and a risk of excessive training. An external mechanical support structure is, therefore, of primary importance for an effective magnet design. The requirements of such a supporting structure can be summarized as:

- increasing the rigidity of the impregnated coil-former assembly to keep the coil stress well below the superconductor degradation limit and to avoid plastic deformation of the formers, and
- minimizing the coils' movement during energization to avoid epoxy cracking or delamination from the channel walls.

To meet the above-mentioned requirements a bladder-and-key type structure with Aluminum shell has been envisioned for

the two PSI model magnets. In Fig. 2, the cross section of this mechanical structure with the two layers of CD1 is shown.

A 4-mm-thick Al protective shell (internal diameter 122 mm) envelops the two coil layers (an 0.2 mm Kapton sheet is wrapped on the protective shell for better electrical insulation to ground). Two symmetric stainless steel pads (78 × 156 mm W × H, with ID of 130.2 mm) surround the coils. The contact surfaces between the pads lie on the (y, z) plane. The iron yoke, which surrounds the pads, is composed of two laminated half yokes, with cut planes at x = ±2.5 mm (opening a gap of 5 mm between them). Horizontal and vertical slots for bladder- and-key insertion are machined into that half yokes. The outer Al shell (internal diameter 500 mm) encloses the whole structure and has a thickness of 25 mm.

The main difference between the above described structure and classical bladder-and-key assemblies concerns the status of the contact surfaces between the pads: In this implementation of bladder-and-key, those contacts must be guaranteed to be closed during all the loading steps, from room temperature through cooldown and magnet operation. This concept was found to achieve an increased rigidity, when compared to the standard open-contact configuration of the pads surrounding the coils. Through the insertion of the horizontal keys between pads and half-yokes at room temperature, the pads' contact surfaces are pre-loaded; vertical keys do not introduce additional compression, but merely limit vertical movement. The slight horizontal pad deformation creates a pre-compression of the coils (squeezed toward the vertical plane). During cool down, the loading increases due to the shrinkage of the external Aluminum shell, which is transferred to the pads via the iron yoke (the two half of the yoke move toward each other and the gap between them is reduced). In this mechanism lies also the reason why stainless steel is used for the pads instead of iron, which would increase the magnetic field; stainless steel has a thermal contraction coefficient closer to that of the coils, and so, less pre-compression on the coils is lost during cool down. Finally, when Lorentz forces act on the coils, the whole structure counteracts the outward horizontal forces; the pad-pad interface is unloaded but, crucially, never opens, thus, ensuring minimal coil movement.

IV. Mechanical Analysis of the CD1 Model Magnet

In Table I the mechanical properties of the materials and their assumed yield stresses are reported (average stress at which a 0.2% permanent strain is observed, referred to in the following as the stress limit), at room temperature and at 4.2 K, respectively. These values are also used by the other three candidate designs for the FCC study, with the exception of the stress limit for the impregnated conductor. We deliberately set 130 MPa, rather than 200 MPa, as the upper bound for cable stress in order to verify that a CCT design with the proposed mechanical structure can provide substantially higher stress margins. Two sets of simulations, using ANSYS finite element software, were carried out. The first is a 2-D analysis of the magnet cross section assuming a plane stress condition. The second is a 3-D periodic model of a slice, using a generalized plane stress axial boundary condition (refer to [12] for a detailed treatment of this topic). The interface regions between the structural components are modeled using several contact conditions. The two coil layers can slide relative to each other with no friction, modelling a dedicated sliding plane in the coil assembly. The same condition is applied to the interface between the protective shell and the outermost coil. The Kapton sheet is considered as bonded to the protective shell. Because the loading of the structure is meant to establish compressive forces on the components of the assembly, contacts can open and no sliding is permitted at the interfaces between the Kapton sheet and the Pads, and between the Yoke and the Al Shell. However, friction has to be taken into account ($\mu = 0.2$) between Yoke and Pads where keys are inserted.

TABLE I
Material Properties and Yield Stress Limits at Room Temperature and at 4.2 K

Material	Stress Limit (MPa) 300 K/ 4.2 K	E (GPa) E300 K/ 4.2 K	ν	$\alpha\,(10^{-3})$
Coil	130(2-D); 150/200 (3-D)	$E_x = 30/33$ $E_y = 25/27.5$ $G_{xy} = 21/21$	0.3	$\alpha_x = 3.1$ $\alpha_y = 3.4$
Stainless Steel	350/1050	193/210	0.28	2.8
Al	480/680	70/70	0.3	4.2
Iron	180/720	213/224	0.28	2.0
Al Bronze	150/400	120/110	0.3	3.12

Each simulation is divided into five load steps: (i) Vertical-bladder inflation and vertical-key insertion (**vert. blad.**); (ii) Vertical-bladder deflation and horizontal-bladder inflation with horizontal-key insertion (**hor. blad.**); (iii) Horizontal-bladder deflation, that is, assembly of the magnet at room temperature (**room temp.**); (iv) Cool-down of the assembly to 1.9 K (**cool down**); (v) Lorentz forces acting on the coils at the **short sample** limit (12 T in the magnet bore at 20 kA). Note that 40 MPa was set as the maximum bladder pressure, and sufficient clearance for the insertion of keys was verified.

A. 2-D Simulations Results

In Fig. 3 at the top, the azimuthal stress distributions for the impregnated cable (left) and the formers (right) at the **short sample** step, using a 0.3-mm horizontal key interference are shown. On the bottom, the maximum Von Mises stress for both, the coils and formers, as a function of the five load steps is shown. It is clear from those figures that the maximum values are well below the stress limits defined in Table I (max. 101 MPa for the coils and max. 272 MPa for the formers at the **short sample** step). The margins in the other components are even larger. Moreover, the contact pressure between the pads is guaranteed during all load steps. To monitor coil movement, Fig. 4 shows the difference of the formers' radial displacement between **cool down** and **short sample** load steps. The arrows indicate the radial movement directions. Along the y-axis, the coil squeezes roughly by 180 μm, while it expands by 140 μm along the x-axis. We deem this scale of movements to be reasonable, not compromising the magnet's performance.

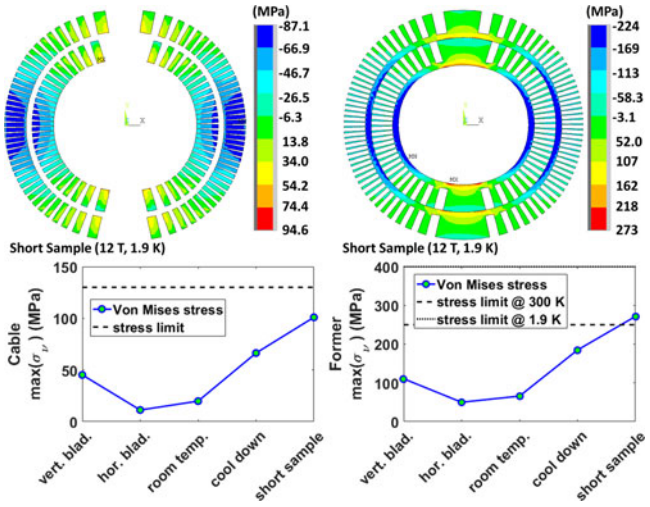

Fig. 3. At the top, azimuthal stress distribution on the impregnated cable (left, $\sigma_\theta = [-87.1, 94.6]$ MPa) and formers (right, $\sigma_\theta = [-224.0, 273.0]$ MPa); on the bottom, maximum Von Mises stress from vertical-bladder-inflation to short-sample load steps for the impregnated cable (left) and former (right).

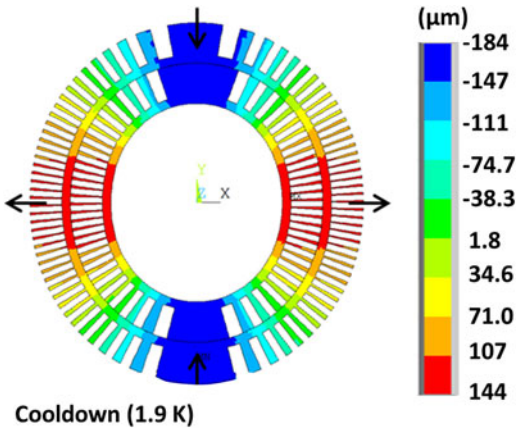

Fig. 4. Difference of the formers radial displacement between **cool down** and **short sample** load steps (units in m).

The above maximum stress values depend on the tolerances on the structural components. The most critical ones that were identified are on (a) the outer radius of the protective Al shell (OR_A) and the inner radius of the pads (IR_P), the size (b) of the horizontal and (c) the vertical keys, and (d) the contact interface between pads. To evaluate the influence of these parameters on the peak stresses, a first parametric scan where each parameter has a ± 100 μm deviation from its nominal value was carried out (using 5 values per parameter interval).

First, each parameter's sensitivity was studied individually, then a two-parameter-at-a-time parametric scan indicated that acceptable tolerances on the aforementioned parameters are: [0, 40] μm for the maximum difference between OR_A and IR_P; ± 50 μm for the keys' sizes; ± 25 μm on the initial distance between the contact interfaces between the pads. To verify the validity of these conclusions, a final parametric scan considered all five parameter at a time (totaling 625 simulations).

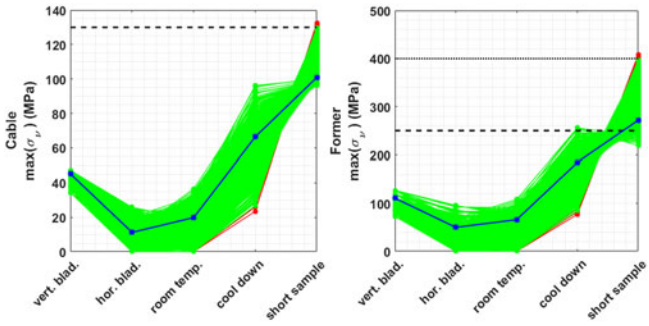

Fig. 5. Maximum Von Mises stress, resulting from the parametric tolerance study, from vertical-bladder inflation to short-sample load steps for the cables (left) and formers (right). The blue curves refer to the reference design (horizontal keys interference of 0.3 mm), the green curves stand for peak stresses below limits (see Table I), and the red ones highlight the condition where limits stress are exceeded; see Table II.

TABLE II
PEAK STRESS RESULTS AT THE SHORT SAMPLE STEP FOR THE FOUR SIMULATION RUNS WITH OUT OF LIMIT RESULTS ALONG WITH THE PARAMETER TOLERANCES (A, B, C, AND D; SEE SECTION IV-A)

a (μm)	b (μm)	c (μm)	d (μm)	Cable (MPa)	Former (MPa)
−40	25	25	25	130.46	
−40	25	50	13	130.11	
−40	27.5	50	13	132.60	407.85
−40	27.5	50	25	131.23	402.36

In Fig. 5, the Von Mises maximum stress on the formers and coils as a function of the load steps for all 625 simulations is shown. Green curves refer to a parameter set for which the stress limits are never exceeded and the pads are always in contact.

The blue curve refers to the nominal design (the baseline) and the red curves stand for a set where one or more stress limits are exceeded.

In Table II the four sets where the stress requirements are not met are reported. At the **short sample** step, the peak stress values are out of bounds by only a few MPa. This confirms the robustness of the design with respect to the acceptable mechanical tolerances.

B. 3-D Simulation Results

Fig. 6 shows the azimuthal stress distribution in the periodic coil slice at the **short sample** step assuming the baseline design. The peak azimuthal tensile stress of 284 MPa occurs in the innermost former and is 9 MPa higher than the value obtained with the 2-D analysis. For the coils, the difference is bigger in terms of compressive stress: −120 MPa versus the −87.1 MPa calculated in the 2-D analysis. The Von Mises stress, which accounts also for longitudinal stress, has a maximum value of 156 MPa on the outer coil. In future work, we will compare this slice simulation with a full 3D analysis to investigate whether this increased value is a spurious result of the generalized-plane stress condition.

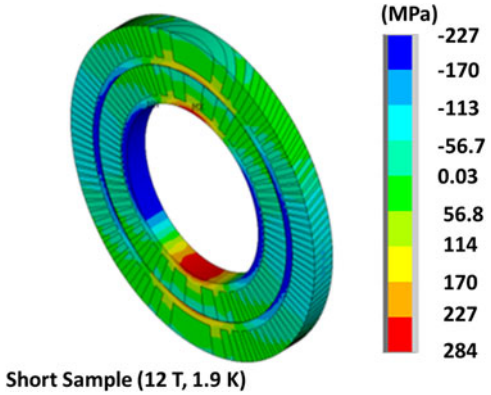

Fig. 6. The azimuthal stress distribution for the periodic coil slice at the **short sample** load step with 0.3 mm horizontal keys interference (baseline design).

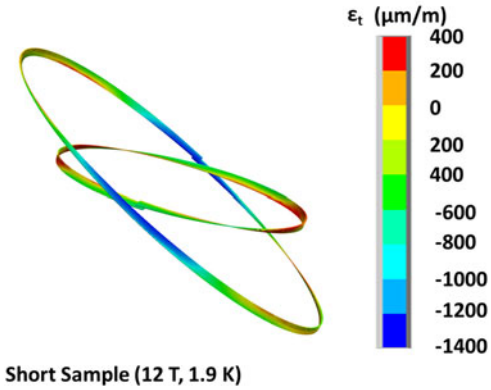

Fig. 7. Strain distribution on coil turns of CD1 at the **short sample** load step. The depicted results are shown with respect to the cable's local reference frame's tangential direction.

The 3-D slice simulations also allow reconstructing stress and strain distributions along a full coil turn (in the local conductor reference frame; compare [12]). In Fig. 7, the strain distribution along the two coil turns on the respective CD1 layers is reported in tangential direction. The peak strain along the cable is 0.04% (400 μm/m). We plan further investigation to estimate the corresponding critical current degradation according to reference values measured in [13].

V. Conclusion

The mechanical structure for the PSI CCT Program has been presented. A detailed 2-D and 3-D (periodic slice model) structural analysis of the first CCT model magnet was carried out. Simulation results show the capability of the designed bladder-and-key structure to keep the stress on the magnet's coil below limit values. Future work is devoted to the production of the first 310-mm-long short mechanical structure. This short-model will allow us to verify results from the mechanical analysis by extensive measurements, followed by the production of the first PSI CCT model magnet.

References

[1] A. Godeke *et al.*, "Limits of NbTi and Nb_3Sn, and Development of W&R Bi–2212 High field accelerator magnets," *IEEE Trans. Appl. Supercond.*, vol. 17, no. 2, pp. 1149–1152, Jun. 2007.

[2] CERN, "The European strategy for particle physics," CERN, Brussels, Belgium, CERN-Council-S/106, 2013.

[3] L. Rossi, "Superconducting magnets for the LHC main lattice," *IEEE Trans. Appl. Supercond.*, vol. 14, no. 2, pp. 153–158, Jun. 2004.

[4] D. Leroy *et al.*, "Design features and performance of a 10 T twin aperture model dipole for LHC," in *Proc. 15th Int. Conf. Magn. Technol.*, Beijing, China, vol. 1, May 1998, pp. 119–123.

[5] D. Tommasini *et al.*, "The 16 T dipole development program for FCC," *IEEE Trans. Appl. Supercond.*, vol. 27, no. 4, Jun. 2017, Art. no. 4000405.

[6] M. Sorbi *et al.*, "The EuroCirCol 16T Cosine–Theta dipole option for the FCC," *IEEE Trans. Appl. Supercond.*, vol. 27, no. 4, Jun. 2017, Art. no. 4001205.

[7] F. Toral, "EuroCirCol 16 T common-coil dipole option for the FCC," *IEEE Trans. Appl. Supercond.*, vol. 27, no. 4, Jun. 2017, Art. no. 4001105.

[8] C. Lerin, D. Durante, and M. Segreti, "EuroCirCol 16 T block-coils dipole option for the future circular collider," *IEEE Trans. Appl. Supercond.*, vol. 27, no. 4, Jun. 2017, Art. no. 4001405.

[9] S. Caspi *et al.*, "The use of pressurized bladders for stress control of superconducting magnets," *IEEE Trans. Appl. Supercond.*, vol. 11, no. 1, pp. 2272–2275, Mar. 2001.

[10] B. Auchmann *et al.*, "Electromechanical design of a 16-T CCT twin-aperture dipole for FCC," *IEEE Trans. Appl. Supercond.*, vol. 28, no. 3, Apr. 2018, Art. no. 4000705.

[11] S. Caspi, "Design of a canted-cosine-theta superconducting dipole magnet for future colliders," *IEEE Trans. Appl. Supercond.*, vol. 27, no. 4, Jun. 2017, Art. no. 4001505.

[12] L. Brouwer, "Canted-cosine-theta superconducting accelerator magnets for high energy physics and ion beam cancer therapy," Ph.D. dissertation, Univ. California, Berkeley, CA, USA, 2015.

[13] E. Barzi, D. Turrioni, and A. V. Zlobin, "Progress in Nb3Sn RRP strand studies and Rutherford cable development at FNAL," *IEEE Trans. Appl. Supercond.*, vol. 24, no. 3, Jun. 2014, Art. no. 6000808.

[14] L. Novitski, "Development of a 15 T Nb_3Sn accelerator dipole demonstrator at Fermilab," *IEEE Trans. Appl. Supercond.*, vol. 26, no. 4, Jun. 2016, Art. no. 4001007.